



Effect of monovalent and divalent ionic environment on the in-lattice nanoparticle-grafted single-stranded DNA

Journal:	<i>Soft Matter</i>
Manuscript ID	SM-ART-08-2021-001171.R1
Article Type:	Paper
Date Submitted by the Author:	03-Nov-2021
Complete List of Authors:	Srivastava, Sunita; Indian Institute of Technology Bombay, Department of Physics Chhabra, Anuj; Indian Institute of Technology Bombay, CRNTS Gang, Oleg; Brookhaven National Laboratory, Center for Functional Nanomaterials

Effect of mono- and multi-valent ionic environments on the in-lattice nanoparticle-grafted single-stranded DNA

Sunita Srivastava,^{1*} Anuj Chhabra² and Oleg Gang^{3,4,5*}

¹Department of Physics, Indian Institute of Technology Bombay, Mumbai, 400076, India

²Center for Nanoscience, Indian Institute of Technology Bombay, Mumbai, 400076, India

³Center for Functional Nanomaterials Brookhaven National Laboratory Upton, NY 11973, USA

⁴Department of Chemical Engineering Columbia University New York, NY 10027, USA

⁵Department of Applied Physics and Applied Mathematics Columbia University New York, NY 10027, USA

Abstract

The polyelectrolyte (PE) chains respond in a complex manner to the multivalent salt environments, and this behavior depends on pH, temperature, and the presence of specific counter ions. Although much work was done to understand the behaviour of free PE chains, it is important to reveal their behaviour on nanoparticle's surface, where surface constraints, particle geometry, and multi-chain environment can affect their behaviour and contribute to particles assembly states. Our work investigates, using in-situ small-angle x-ray scattering (SAXS), the morphology of PEs (single-stranded DNA) chains grafted onto a surface of spherical gold nanoparticles assembled in a lattice in the presence of monovalent, divalent and trivalent salts. For divalent salts, the DNA brush length was found to decrease at a faster rate with salt concentration than in the monovalent salt environment, while trivalent salt lead to a chain collapse. Using a power law analysis and modified Daoud-Cotton model, we have obtained insight into the mechanism of nanoparticle-grafted chain's response to ionic environments. Our analysis suggests that the decrease in a brush length is due to the conventional electrostatic screening for monovalent systems, whereas for divalent systems both, electrostatic screening and divalent ion bridging must be considered.

Introduction:

Polyelectrolyte (PE) polymers, with positive or negative charges on their backbones, are known to behave differently under different environmental conditions, such as pH, salt concentration, temperature, nanoparticle environments, and other factors¹⁻³. The previous research showed that modulating environments of the PEs is a powerful way to control their conformations⁴ and stiffness⁵, and it can be used in a variety of applications, for example, in gene and drug delivery^{6,7}, removal of pollutants from the environment⁸, diagnostics⁹ and manipulating nanoparticle assembly¹⁰. The key parameters affecting the PE's chain morphology are salt concentration and salt type¹¹⁻¹². With the increase of salt concentration, the end-to-end distance of the PE chain decreases¹³ due to the reduced electrostatic repulsion between monomers which in turn decreases the persistence length. Divalent and trivalent salts are found to reduce the length of the PEs even more effectively compared to the monovalent salt due to the larger screening and the additional ion-bridging effect¹²⁻¹³.

Single-stranded (ss) DNA is a polyelectrolyte whose backbone is negatively charged due to the phosphate group, yielding a one-unit charge per 0.17 nm. The persistence length of ssDNA chain depends on the ionic strength of the added salt in the surrounding environment¹⁴. Studies suggest that cations such as Na⁺, K⁺, Mg²⁺ etc, typically present in biological systems, can effectively attach to the DNA backbone and modify an interaction of DNA monomers¹⁵⁻¹⁶. In the presence of multivalent salt and higher salt concentration, DNA condensation may also take place¹⁷. Mg²⁺ ions are abundant in biological systems; thus, it is important to understand their effect on the DNA. Mg²⁺ can also promote the binding of pharmaceutically relevant molecules to the DNA; thus, it is important in drug delivery applications⁷. Many studies were conducted to understand the effect of salt concentration and cation valence on the PE chain conformations^{11-13, 18-20}. The work by Chen et al, investigated the flexibility and conformation of nucleic acid using SAXS and smFRET measurements and reported that the screening efficiency of divalent salt is significantly larger than in monovalent salt environments for both ssRNA and ssDNA²¹. However, when these PEs are attached to the nanoparticle surface, high curvature, inter-chain effects, and local constraints add complexity; thus, a detailed study on the effect of cation environment on the behaviour of nanoparticle-grafted PE is required.

The question about the state of PE shell was investigated for curved surfaces²²⁻²³, but the ability to form a well-defined nanoscale system provides an opportunity to study a chain

behaviour and involved interactions at the nanoscales in detail and for different regimes²⁴. In this respect, such a PE system as DNA-grafted nanoparticles are particularly useful due to the exquisite control over a chain length, grafting density of chains, and particle diameter. DNA-mediated nanoparticles systems are promising for programmable material assembly²⁵⁻²⁷, and understanding the chain behaviour in ionic environment is critical for controlling an assembly processes and manipulating interparticle distances^{25, 28-30}. Moreover, this question also becomes highly relevant when DNA origami is employed for nanoparticle organizations³¹⁻³² due to magnesium required for DNA origami stability³³⁻³⁴.

DNA-coated nanoparticles attracted much attention as building blocks for controlling nanomaterials assembly using DNA-programmable interactions³⁵⁻³⁷. A specifically defined complementary ssDNA sequence can form stable bonds via Watson-Crick (WC) base pairing, resulting in double-stranded (ds) DNA. This stable base pairing can be utilized to prescribe interparticle binding through a combination of DNA shell designs on nanoparticles, nanoparticle sizes and by the use of different DNA linking motifs, variety of self-assemble lattices can be formed³⁷⁻⁴⁰. Different types of DNA crystal lattices and control of their dynamic behaviour were shown through a design of the DNA shells, where the enthalpic and entropic contributions were balanced in a specific way⁴¹⁻⁴³. Molecular dynamics simulations have shown that for densely grafted DNA gold nanoparticles, long-range attractions can be induced at the higher salt concentration environments²⁴. This reduction in electrostatic repulsion and increase in long-range attraction can lead to stable macroscopic crystals. In a high salt environment, even without Watson Crick base-pairing, a macroscopic self-assemble structure can be formed⁴⁴. Different models such as DLVO theory⁴⁵, liquid crystal theory, Daoud-Cotton model⁴⁶ have been applied to understand the effect of salt concentration on the PEs. The DNA-AuNP self-assembly has previously been reported to study the effect of salt concentration^{44, 47}, pH^{3, 48}, controllability of the superlattice, etc. Previously reported work by Luo's group has used a combination of SAXS experiment and Daoud-Cotton model to understand the effect of DNA coated nanoparticles in a 2D system and reveal the effect of salt concentration on the DNA chains⁴⁴.

The present work focuses on understanding the behaviour of DNA chains on spherical nanoparticles at monovalent and divalent salt environments when particles are assembled in 3D lattices via DNA hybridization; we also compare these behaviors with a trend observed for a trivalent salt environment. Thiol modified DNA chains were used for the gold nanoparticle functionalization, following their assembly into 3D lattices²⁶. We applied a

synchrotron based in-situ small angle x-ray scattering (SAXS) method to systematically investigate the behaviour of DNA chains grafted on nanoparticle (NP) surfaces by studying changes in lattices at the different salt environments.

Materials and Methods:

Thiol modified DNA chains (purchased from IDT) were used to functionalize gold nanoparticles (AuNP) of size ~10 nm and 15 nm (purchased from Ted Pella). The details of the oligonucleotides are given in Table S1. In a typical functionalization process, the DNA and gold nanoparticles are mixed in the stoichiometric ratio of 100: 1, followed by incubation for about 8 hrs. The Phosphate Buffer (PB) of the desired volume is added to adjust the pH of the solution to about 7.4. NaCl salt was added incrementally to reach a final concentration of ~ 0.2M, which is required for achieving a high DNA grafting density on nanoparticle surface. This procedure was followed by a centrifugation process for purification to remove the free chains. The DNA grafted nanoparticles have been characterized by UV-Vis and zeta potential measurements.

For our salt-dependent studies, three DNA chain length systems (denoted here as sys *A*, *B*, and *C*) have been prepared with the corresponding 35, 50, and 65 nucleotides (monomers) per ssDNA chain. Out of the total number of nucleotides in an ssDNA chain in each system, 15 bases were utilised for the inter-chain hybridization to promote inter-particle bindings. The complementary sequences design is described in Supplementary Material (TS1). To form a self-assemble structure, nanoparticles functionalized with complementary DNA chains were mixed in the 1:1 molar ratio at room temperature. These samples were further annealed for 2 hours at few degrees above the DNA melting temperature to facilitate formation of the maximum number of complementary bonds between nanoparticles and to promote a superlattice assembly.

The monovalent (NaCl), divalent (MgCl₂) and trivalent ([Co(NH₃)₆]Cl₃) salts of 99% purity were purchased from Sigma Aldrich and used by making solutions of desired concentration in 10mM phosphate buffer, pH 7.4. The ionic strength for NaCl was varied from 0.05 M to 0.7 M, and for MgCl₂, the ionic concentration in the range of 0.015 M to 0.21 M was used in our studies.

The *in-situ* structural morphology studies of DNA-AuNP superlattices were performed using high-resolution synchrotron based Small Angle X-ray Scattering (SAXS) technique (X9

beamline of National Light Source, wavelength, $\lambda=0.918 \text{ \AA}$, wavevector in the range of $0.005 \text{ \AA}^{-1} < q < 0.13 \text{ \AA}^{-1}$). Samples with crystalline aggregates of DNA-NP assemblies at varying concentrations of added salts were sealed in quartz capillaries to avoid any error in salt concentration due to solvent evaporation. The structure factor $S(q)(= I(q)/F(q))$ was calculated from the measured x-ray scattering intensity profiles, $I(q)$, obtained by integration of the calibrated CCD images. $F(q)$ is a nanoparticle form factor obtained from measuring the scattering intensity of dispersed DNA-AuNP, and q is a wave vector.

Results and Discussions:

We show in Figure 1a, a schematic representation of the lattice response due to the changes in the nanoparticle shells of polyelectrolyte chains (DNA chains in our studies) upon the addition of monovalent and divalent salt. The DNA chains are expected to show a more significant reduction in divalent salt environments than in monovalent environments, hence resulting in the smaller size of the unit cell in the DNA-NP lattice. For example, we show structure factors, $S(q)$, extracted from the SAXS data, for *Sys B* at various concentrations of divalent salt (MgCl_2) in Fig 1b. The presence of multiple peaks in the ratio of 1, $\sqrt{2}$, $\sqrt{3}$, 2, $\sqrt{5}$, and so on, indicates the formation of assembly with a long-range order, where NPs are arranged in closed packed body-centered cubic (BCC) lattice. Inter planar distances, d was calculated from the first peak position of the $S(q)$ as $d = 2\pi/q^1$, where q^1 is the position of the first-order peak of the structure factor. The center-to-center AuNP distance was obtained as, $a = d\sqrt{2}$. In this case a half of the surface-to-surface distance provides an estimation on the DNA brush length, H ($H = (a-10)/2 \text{ nm}$), for DNA chains grafted onto a surface of the 10 nm NPs arranged in the BCC lattice (Fig 1a). This approximation does not account for the formation of double helix part due to WC pairing due to more complex conformations of grafted chains in a lattice arrangement. Thus, in this study, we use H as an effective measure of DNA brush length in a NP shell.

The data in Figure 1b indicate a shrinkage of the nanoparticle lattice due to a brush thickness decrease upon an increase of ionic strength for added salt, as evident from a position shift of the scattering peaks in $S(q)$ towards higher q . Qualitatively similar behaviour was observed for all studied systems (*A*, *B*, and *C*) when concentrations of monovalent (NaCl) and divalent (MgCl_2) salts were increased. However, the detailed comparison, as we discuss below, demonstrates that H decreases stronger with salt concentration increase for divalent salt than

for the monovalent case. We further compare these observations with the behavior in a trivalent salt.

The estimates of the DNA chain length, H , at varying ionic strength, C_s , of monovalent and divalent salts, for all the systems, are shown in Figure 2a, b, respectively. The estimates of ionic strength were obtained using, $C_s = \frac{1}{2} \sum_{i=0}^n C_i z_i^2$, where C_i and z_i , are molar salt concentration and charge of the i^{th} ion, respectively. It is to be noted that in order to achieve the H comparable to the highest monovalent concentrations ($\sim 0.8\text{M}$), an order of magnitude lower concentration is required for the divalent salt. For example, the estimate of H for *Sys A*, *Sys B*, and *Sys C*, at added ionic strength of monovalent salt of 0.05 M is 7.2 nm , 9.5 , and 12.2 nm , respectively, whereas, at similar ionic strength (0.06M) of divalent salt, the corresponding estimates were found to be 4.2 nm , 6.4 nm , and 8.1 nm respectively. This indicates that the decrease in chain length is larger by ~ 71 , 48 , 51% , respectively, for divalent vs monovalent salt, and the corresponding change in DNA-NP lattice by volume is 133 , 105 , 126% .

To quantify the change of a DNA chain length with salt, we have performed analysis by fitting the H vs C_s data to $\sim C_s^{-\alpha}$ form of power-law decay, where α is the decay exponent as shown in Figure 2a,b. Interestingly, we find the estimate of α is independent of the DNA system and depends on monovalent and divalent salts. The average values of α , for monovalent and divalent salt environments, were estimated to be $\sim 0.13 \pm 0.01$ and 0.24 ± 0.012 , respectively, thus indicating approximately two-fold larger exponent for the divalent systems. The obtained value of α for the studied DNA-NP systems in a monovalent cation environment is in accordance with the previously reported values (~ 0.14) by Hariharan et al²³, for PE chains grafted on spherical polystyrene particles. The nearly doubling of α for divalent cations indicates that a more complex phenomenon might be controlling the length of chains brush.

The addition of monovalent salt in case of free PEs in solution leads to a dependence that scales as $H \sim C_s^{-0.1}$, which can be primarily understood by the electrostatic interactions of the monovalent salt with the PEs monomers⁴⁹. Previous reports have shown that not only the type of cation but the geometry of the chains, for example, free chains in bulk^{14, 49-51}, surface grafted chains as planar brushes^{23, 52-55}, or star polymers^{46, 56} can play a significant role in defining the chain morphology in the presence of the counterions. In the case of a neutral polymer chains tethered to planar surfaces, the scaling of the brush length, H , with C_s is given

as, $H \sim kNa(\sigma)^{1/3} C_s^{-\alpha}$, N is the number of monomers, a is the monomer size and σ is the grafting density. In the case of a planar brush, the expected value of $\alpha \sim 0.33$, as reported experimentally⁵² and theoretically⁵⁷. To test the applicability of the planar brush model to our system, we first attempted to fit our data with a planar brush model (Fig S3). As evident from the analysis (Supplementary Material), this model is unable to capture the dependence of H on C_s . This suggests that the modified Daoud-Cotton model, which incorporates the curvature effect on the polymer chain morphology, might be more appropriate in this case.

Hence, we have applied a modified Daoud-Cotton model that was developed to explain the morphology of star polymers⁴⁶. This model allows us to understand the effect of excluded volume, the number of nucleotides, and chain density on polyelectrolyte chain morphology. However, this model cannot be directly used to assess the structural morphology of grafted PEs on spherical surfaces, as it does not account for the curvature effects. Further, Zulina⁵⁶ and Hariharan et al.²³ modified the original Daoud-Cotton model⁴⁶ to include the electrostatic and surface curvature effects. Since the excluded volume of the PE chain depends in a complex manner on the ionic strength, this effect should be considered explicitly. The electrostatic effect on excluded volume parameters was further incorporated (Section IV of Supplementary Material), and the corresponding PE brush length is described by the following equation⁴⁴,

$$\frac{H}{R} + 1 = \left[1 + \frac{C_s^{-\alpha_1/3} K N^{(3-\beta_1)/3} a}{R} (\sigma)^{\frac{1-\beta_1}{3}} \right]^{\frac{3}{5}} \quad [1]$$

where R is the radius of spherical surface (nm), K is the scaling constant is close to 1 and 0.5 for monovalent salt and divalent salt respectively, N is the number of nucleotides (monomers), a is the monomer size (nm), and σ is the grafting density (nm⁻²) of the DNA chain on a nanoparticle surface. For 10 nm particle, the grafting density is ~ 0.22 nm⁻², corresponding to approximately 70 DNA chains per particle. The exponent, α_1 and β_1 , are the fitting parameters for determining the scaling of the DNA brush length on C_s and N , respectively, as given in equation 1.

We applied the equation 1, to fit the experimental data and the fit results for monovalent and divalent cases are presented in Fig. 2c and Fig. 2d, respectively. The fit to our data using this modified Daoud-Cotton model (Eq. 1) provides insight into the interactions of counterions with the DNA chains. In our analysis, the value of exponent β_1 is fixed to 0, according to the

scaling relation ($H \sim N^{3/5}$) for polymer chains for good solvent^{45, 58}. Additionally, we also verified the fit parameters by considering a poor solvent condition for DNA chain morphology (Section V of Supplementary Material). We find that although we can fit the data, the fit-estimated N is much higher than a real (designed) value, indicating that the assumption of poor solvent is not valid here. The parameters obtained from the fit are summarized in the table TS4. The general applicability of the model was tested by performing the fit to our data using Eq.1 by allowing to vary the known parameters such as R , N , β_l , as discussed in detail in Section VI of Supplementary Material. This, however, results in larger errors, therefore, all our fit was performed at the fixed values of the known parameters. The values of α_l obtained from a fit is independent of the DNA chain length, and they approximately equal to 0.56 ± 0.03 and 0.96 ± 0.05 for monovalent and divalent salt, respectively. The Daoud-Cotton model and the power-law analysis provides us with the corresponding estimates of α ($= \frac{\alpha_1}{5}$) ~ 0.11 and ~ 0.13 for monovalent salt, while for divalent salt the α values are correspondingly ~ 0.20 and ~ 0.24 . The power-law analysis and the discussed modified Daoud-Cotton model fit indicate that the divalent cations might contribute to the decrease in chain length not only through the screening mechanism, but the additional ion-mediated effect might be considered. This effect is responsible for a higher value of α and hence stronger dependences of DNA chain length on divalent salt concentration. Two major effects that might contribute to this behaviour, overcharging of the DNA chain backbone by the divalent ions¹²⁻¹³ and attraction between like-charged polyelectrolytes leading to ion-bridging^{16, 59-60}.

Overcharging is a phenomenon reported for charged PEs in the presence of a high concentration of divalent cations^{12-13, 61}. In such a scenario, the initial decrease in PE chain length due to the screening of electrostatic repulsion is followed by an increase in length due to interchain repulsion from overcharging that occurs due to adsorbed cations. Indeed, it has been observed for free ssDNA that at intermediate concentrations of divalent salts, the cations initially neutralize the charge on PEs¹². Further increase in a divalent salt concentration leads to overcharging on the PE backbone via adsorption of the divalent cations, resulting in repulsion between the monomers of the chains. The overcharging phenomenon is accompanied by a signature of non-monotonic change in the dependence of PE chain length on a salt concentration^{13, 19, 61}. In contrast to free DNA chains, no upturn was observed for H vs C_s dependence in our experiments, even at the highest divalent salt concentration, thus indicating no evidence of overcharging for DNA-NP systems. This observation suggests that

for DNA shell of grafted chains a non-specific coupling between added cations and DNA chain backbone, not-only screens the like charge repulsion but also induces an attraction within and between DNA chains in the case of divalent salt. In literature such attraction were found to occur due to non-specific binding of the multivalent cations to the closely packed phosphate backbone for double stranded DNA⁶² and branched DNA structures^{63, 59, 64}. To the best of our knowledge, the ion-bridging mediated attraction phenomenon is observed for double-stranded DNA with cation valency > 2 ⁶⁵ or salt ions with non-linear structure^{60, 65}. We have further compare the observed effects with the behaviour in the trivalent salt ($[\text{Co}(\text{NH}_3)_6]\text{Cl}_3$). For our DNA-NP system, we find that the trivalent salt is very effective in screening the electrostatic repulsion (Section VIII in Supplementary Material). Overcharging is predominately observed for salts with valency ≥ 3 ^{12, 20}. For the discussed DNA-NP system, we do not observe the evidence of the overcharging effect for trivalent salt: DNA chains were found to collapse at very low C_s of 2.4 mM DNA and remain at this conditions for higher C_s (Fig. S5). The previous studies suggest that the monovalent and non-specifically binding divalent cations cannot induce the aggregation of double-stranded DNA. To observed DNA condensation using divalent salts, dsDNA chains with specific sequence⁶⁴, triple-stranded DNA chains⁶⁶ are required for enhanced attraction between closely spaced phosphate backbones wherein cations bind and mediate attraction via ion bridging⁶⁶.

It is interesting to note that the DNA-NP systems in our studies primarily constitute single-stranded DNA, with the dsDNA components of $\sim 33\%$, 18% , and 13% for *sys A*, *B*, and *C*, respectively. Even for *sys C*, with the smallest composition of dsDNA (13%), a strong effect of divalent cation is observed. We measured an approximately two-fold decrease of DNA brush length in the presence of added divalent salt compared to a monovalent salt. It is well known that divalent cations attract to the DNA phosphate backbone stronger than monovalent ones, and this, through the reduced repulsions between monomers, can result in a decrease of a chain length¹⁶. Mg^{2+} ions are found to reside in the pockets formed by the phosphate backbone, but at the same ionic strength, Na^+ ions do not bound to the phosphate backbone as strongly as Mg^{2+} ions^{60, 62, 64}. We propose that the divalent mediated ion-bridging effect in our system (which is primarily ssDNA) is due to the high density of DNA chains on a nanoparticle surface, and this can effectively facilitate both inter-and intra- DNA chain interactions leading to cation mediated attraction. A similar effect of divalent salt on DNA-chain length was observed for DNA coated NPs assembly at air-water interface⁴⁴. Our study

suggests that divalent salt mediated ion-bridging can also be observed for ssDNA chains in high density environments.

To further quantify the DNA chain response to salt, the difference between the brush length, $\Delta H = (H_{monovalent} - H_{divalent})$, for monovalent and divalent salts at same ionic strength, is plotted in Fig 3. The estimate of ΔH increases at the low salt concentration and then saturates at the specific ionic strength, C_s^* . All the studied systems exhibit this behaviour. To quantify the value of C_s^* , we have used an exponential growth function (Supplementary Material) to fit the experimental $\Delta H(C_s)$ dependence, which yields $C_s^* \sim 0.07 M$, $0.11 M$, and $0.16 M$ for sys *A*, *B*, and *C* respectively. It is evident that the estimation of C_s at which ΔH saturates is shifted towards a higher value, indicating that a saturation ionic strength, C_s^* , depends on the number of monomers per DNA chain.

Considering the number of grafting chains, approximately 70 chains/particle for all studied systems, we find that the negative charge density is about $6.7 e/nm^2$, $11.1 e/nm^2$, and $14.4 e/nm^2$ for the sys *A*, sys *B*, and sys *C*, respectively. As a number of nucleotides increases in a DNA chain, there is an increase in charges per unit area; thus, a larger number of cations are required to neutralize DNA chains. Moreover, for longer DNA chains, a larger number of Mg^{2+} ions is required to form the same number of bridges. Therefore, this explains why we observe an upshift in the saturation value of ΔH as the number of monomers per DNA chain increases.

We propose that for our systems two effects, the ion bridging and the electrostatic screening, might be responsible for the observed behaviour. The electrostatic screening is present for all ranges of salt concentrations for both monovalent and divalent cases. For monovalent scenarios, both the power-law exponent and Daoud-Cotton model fittings, suggest that the change in DNA brush length can be understood by the screening of electrostatic repulsions. However, for a divalent system, one needs to consider the overlaying effect of ion-bridging as well. The data presented in Figure 3 suggests that at the low ionic strength both the ion-bridging and charge screening are contributing, which leads to the greater decrease of the brush length for a divalent salt. For the higher ionic strength, an ion-bridging saturates, and only charge screening effect occurs, leading to the saturation of the ΔH at these salt concentrations. Since the ion bridging occurs within an ssDNA backbone, it is expected to depend on the number of monomers per chain. For shorter chains, fewer bridges are formed;

thus, a saturation point will occur at the lower C_s compared to longer chains, as evident from the data shown in Figure 3.

To further understand the effect of ion-bridging for DNA chains grafted to a spherical nanoparticle, we have investigated an AuNP system with a larger, 15 nm nanoparticle core diameter, which was functionalized with DNA used for *sys B*. With an estimate of ~ 70 and 100 DNA chains per 10 nm and 15 nm particles⁶⁷, we calculated $\sim 63\%$ decrease in grafting density. Owing to the curvature effect, the DNA chain on 15 nm AuNP is expected to adapt less extended morphology compared to the 10 nm system. The power-law analysis for systems with 15 nm core NP at various concentrations of monovalent and divalent salts is shown in Figure 4a. For added NaCl, 15 nm AuNP exhibits a power-law exponent, $\alpha = 0.14$, close to the exponent for 10 nm systems (~ 0.12). However, the $H(C_s)$ dependence for MgCl_2 exhibits two different slopes: in the low salt concentration regime, α is about 0.29 , followed by a change in slope to $\alpha \sim 0.15$ at $C_s \sim 0.2\text{ M}$, close to a value observed for NaCl case. Beyond 0.2 M , the lower exponent (also plotted on a linear scale (Fig S5b), indicates that ion-bridging is maximized. At these concentrations, chains adopt a mushroom-like conformation and are pinned stronger to the nanoparticle surface. The schematic of the proposed mechanism for the observed change for DNA brush is shown in Figure 4b.

In summary, we report the behaviour of nanoparticle-grafted DNA chains in a divalent (Mg^{2+}) salt environment that indicates an ion-bridging mediated attraction of chains. Our experimental results and analysis suggest that the ion bridging and the electrostatic screening effects are primarily the major factors driving the morphology of DNA chains on nanoparticle surfaces. For the monovalent salt, the change in DNA brush thickness is mainly determined by the electrostatic screening of monomers; however, for the divalent salt, our data suggest the effect of ion bridging, thus, leading to about doubling of the power-law exponent. The chain collapse was observed at the low concentration of trivalent salt, and it remained for all higher concentrations. The data for all studied system does not indicate the presence of the overcharging effect, even at the high salt concentrations. This observation is further confirmed by altering the chain grafting density, where the ion-bridging and the electrostatic screening can be correspondingly observed at the low and high divalent salt concentrations.

Conclusion:

This work investigates the behaviour of polyelectrolyte chains (ssDNA) grafted onto nanoparticle surfaces in the presence of monovalent and divalent cations. The salt-dependent morphology of the DNA chain is found to follow a modified Daoud-Cotton model. With a salt concentration increase, the thickness of the DNA shell decreases for both monovalent and divalent salts. While for the monovalent salt, the change in DNA chain length can be rationalized by an electrostatic screening, the behaviour of systems in divalent salt solutions can be explained through both electrostatic screening and inter- and intra-chain ion bridging effects. Previously, an ion-bridging mediated attraction was observed for dsDNA with cation valency greater than 3. Using trivalent salt, $[\text{Co}(\text{NH}_3)_6]\text{Cl}_3$, we find that the chain collapse occurs at a low (micromolar range) salt concentration, indicating strong effect of trivalent salt on DNA brush length. The tertiary DNA chains or dsDNA with specific sequences were found to exhibit DNA chain attraction mediated via ion bridging in divalent salt environments. Our experimental results reveal that divalent cations can mediate an ion-bridging for systems constituting primarily ssDNA compositions. Thus, through our experiments, we demonstrate that DNA condensation can occur in systems of high-density particle-grafted DNAs in divalent environments.

Acknowledgment

AC acknowledges financial support from CRNTS, IITB. SS acknowledges support from Ramanujan Fellowship (SB/S2/RJN-094/2014) and ECR-SERB (ECR/2017/003104), DST, India. We thank SAIF-IITB for the use of the Small Angle X-ray facility. OG was supported by the US Department of Energy, Office of Basic Energy Sciences, grant DE-SC0008772. This research used resources of the Center for Functional Nanomaterials and National Synchrotron Light Source II, supported by U.S. DOE Office of Science Facilities at Brookhaven National Laboratory under Contract No. DE-SC0012704.

References:

1. Rudiuk, S.; Yoshikawa, K.; Baigl, D. J. J. o. c.; science, i., Enhancement of DNA compaction by negatively charged nanoparticles: Effect of nanoparticle size and surfactant chain length. **2012**, *368* (1), 372-377.
2. Meka, V. S.; Sing, M. K.; Pichika, M. R.; Nali, S. R.; Kolapalli, V. R.; Kesharwani, P., A comprehensive review on polyelectrolyte complexes. *Drug Discov Today* **2017**, *22* (11), 1697-1706.
3. Srivastava, S.; Fukuto, M.; Gang, O., Liquid interfaces with pH-switchable nanoparticle arrays. *Soft Matter* **2018**, *14* (19), 3929-3934.

4. Estévez-Torres, A.; Baigl, D. J. S. M., DNA compaction: fundamentals and applications. **2011**, *7* (15), 6746-6756.
5. Innes-Gold, S. N.; Jacobson, D. R.; Pincus, P. A.; Stevens, M. J.; Saleh, O. A., Flexible, charged biopolymers in monovalent and mixed-valence salt: Regimes of anomalous electrostatic stiffening and of salt insensitivity. *Phys Rev E* **2021**, *104* (1), 014504.
6. Ewert, K. K.; Zidovska, A.; Ahmad, A.; Bouxsein, N. F.; Evans, H. M.; McAllister, C. S.; Samuel, C. E.; Safinya, C. R., Cationic Liposome–Nucleic Acid Complexes for Gene Delivery and Silencing: Pathways and Mechanisms for Plasmid DNA and siRNA. In *Nucleic Acid Transfection*, Bielke, W.; Erbacher, C., Eds. Springer Berlin Heidelberg: Berlin, Heidelberg, 2010; pp 191-226.
7. Sreedhara, A.; Cowan, J., Structural and catalytic roles for divalent magnesium in nucleic acid biochemistry. *Biomaterials* **2002**, *15* (3), 211-223.
8. Zinchenko, A. A.; Sakai, H.; Matsuoka, S.; Murata, S., Application of DNA condensation for removal of mercury ions from aqueous solutions. *J Hazard Mater* **2009**, *168* (1), 38-43.
9. Oh, J.-H.; Lee, J.-S., Salt concentration-induced dehybridisation of DNA–gold nanoparticle conjugate assemblies for diagnostic applications. *Chem Commun* **2010**, *46* (34), 6382-6384.
10. Zhang, H.; Wang, W.; Mallapragada, S.; Travesset, A.; Vaknin, D., Macroscopic and tunable nanoparticle superlattices. *Nanoscale* **2017**, *9* (1), 164-171.
11. Wang, L.; Bloomfield, V. A. J. M., Small-angle x-ray scattering of semidilute rodlike DNA solutions: polyelectrolyte behavior. **1991**, *24* (21), 5791-5795.
12. Wang, F. H.; Wu, Y. Y.; Tan, Z. J., Salt contribution to the flexibility of single-stranded nucleic acid of finite length. *Biopolymers* **2013**, *99* (6), 370-381.
13. Ghosh, S.; Dixit, H.; Chakrabarti, R. J. C. P., Ion assisted structural collapse of a single stranded DNA: A molecular dynamics approach. **2015**, *459*, 137-147.
14. Tinland, B.; Pluen, A.; Sturm, J.; Weill, G., Persistence length of single-stranded DNA. *Macromolecules* **1997**, *30* (19), 5763-5765.
15. Gelbart, W. M.; Bruinsma, R. F.; Pincus, P. A.; Parsegian, V. A., DNA-inspired electrostatics. *Physics today* **2000**, *53* (9), 38-45.
16. Allahyarov, E.; Gompper, G.; Lowen, H., Attraction between DNA molecules mediated by multivalent ions. *Phys Rev E* **2004**, *69* (4).
17. Muthukumar, M., Theory of counter-ion condensation on flexible polyelectrolytes: adsorption mechanism. *J Chem Phys* **2004**, *120* (19), 9343-50.
18. de La Cruz, M. O.; Belloni, L.; Delsanti, M.; Dalbiez, J.; Spalla, O.; Drifford, M. J. T. J. o. c. p., Precipitation of highly charged polyelectrolyte solutions in the presence of multivalent salts. **1995**, *103* (13), 5781-5791.
19. Sarkar, S.; Maity, A.; Sarma Phukon, A.; Ghosh, S.; Chakrabarti, R. J. T. J. o. P. C. B., Salt induced structural collapse, swelling, and signature of aggregation of two ssDNA strands: insights from molecular dynamics simulation. **2018**, *123* (1), 47-56.
20. Hsiao, P.-Y. J. M., Chain morphology, swelling exponent, persistence length, like-charge attraction, and charge distribution around a chain in polyelectrolyte solutions: effects of salt concentration and ion size studied by molecular dynamics simulations. **2006**, *39* (20), 7125-7137.
21. Chen, H.; Meisburger, S. P.; Pabst, S. A.; Sutton, J. L.; Webb, W. W.; Pollack, L., Ionic strength-dependent persistence lengths of single-stranded RNA and DNA. *P Natl Acad Sci USA* **2012**, *109* (3), 799-804.
22. Biver, C.; Hariharan, R.; Mays, J.; Russel, W. B., Neutral and charged polymer brushes: a model unifying curvature effects from micelles to flat surfaces. *Macromolecules* **1997**, *30* (6), 1787-1792.
23. Hariharan, R.; Biver, C.; Mays, J.; Russel, W. B., Ionic Strength and Curvature Effects in Flat and Highly Curved Polyelectrolyte Brushes. *Macromolecules* **1998**, *31* (21), 7506-7513.
24. Kewalramani, S.; Guerrero-García, G. I.; Moreau, L. M.; Zwanikken, J. W.; Mirkin, C. A.; Olvera de la Cruz, M.; Bedzyk, M. J., Electrolyte-Mediated Assembly of Charged Nanoparticles. *ACS Central Science* **2016**, *2* (4), 219-224.

25. Gang, O.; Kahn, J., Designer Nanomaterials through Programmable Assembly. *Angewandte Chemie International Edition* **2021**, *n/a* (n/a).
26. Nykypanchuk, D.; Maye, M. M.; van der Lelie, D.; Gang, O., DNA-guided crystallization of colloidal nanoparticles. *Nature* **2008**, *451* (7178), 549-52.
27. Park, S. Y.; Lytton-Jean, A. K. R.; Lee, B.; Weigand, S.; Schatz, G. C.; Mirkin, C. A., DNA-programmable nanoparticle crystallization. *Nature* **2008**, *451* (7178), 553-556.
28. Zhang, H.; Wang, W.; Hagen, N.; Kuzmenko, I.; Akinc, M.; Travesset, A.; Mallapragada, S.; Vaknin, D., Self-Assembly of DNA Functionalized Gold Nanoparticles at the Liquid-Vapor Interface. *Adv Mater Interfaces* **2016**, *3* (16), 1600180.
29. Laramy, C. R.; O'Brien, M. N.; Mirkin, C. A., Crystal engineering with DNA. *Nature Reviews Materials* **2019**, *4* (3), 201-224.
30. Seo, S. E.; Girard, M.; de la Cruz, M. O.; Mirkin, C. A., The Importance of Salt-Enhanced Electrostatic Repulsion in Colloidal Crystal Engineering with DNA. *Acs Central Sci* **2019**, *5* (1), 186-191.
31. Ye Tian, J. R. L., Lin Bai, Thi Vo, Huolin Xin, Huilin Li, Ruipeng Li, Masafumi Fukuto, Kevin G. Yager, Jason S. Kahn, Yan Xiong, Brian Minevich, Sanat K. Kumar, Oleg Gang, 3D-Organized Nanomaterials through DNA-prescribed and Valence-controlled Material Voxels. *Nature materials* **2020**, *19*, 789-796.
32. Liu, W.; Tagawa, M.; Xin, H. L.; Wang, T.; Emamy, H.; Li, H.; Yager, K. G.; Starr, F. W.; Tkachenko, A. V.; Gang, O., Diamond family of nanoparticle superlattices. *Science* **2016**, *351* (6273), 582 LP-586.
33. Kielar, C.; Xin, Y.; Shen, B.; Kostianen, M. A.; Grundmeier, G.; Linko, V.; Keller, A., On the Stability of DNA Origami Nanostructures in Low-Magnesium Buffers. *Angewandte Chemie International Edition* **2018**, *57* (30), 9470-9474.
34. Wang, S.-T.; Gray, M. A.; Xuan, S.; Lin, Y.; Byrnes, J.; Nguyen, A. I.; Todorova, N.; Stevens, M. M.; Bertozzi, C. R.; Zuckermann, R. N.; Gang, O., DNA origami protection and molecular interfacing through engineered sequence-defined peptoids. *Proceedings of the National Academy of Sciences* **2020**, *117* (12), 6339-6348.
35. Tian, Y.; Zhang, Y.; Wang, T.; Xin, H. L.; Li, H.; Gang, O., Lattice engineering through nanoparticle–DNA frameworks. *Nature materials* **2016**, *15* (6), 654-661.
36. Xiong, H.; van der Lelie, D.; Gang, O., Phase Behavior of Nanoparticles Assembled by DNA Linkers. *Phys Rev Lett* **2009**, *102* (1), 015504.
37. Macfarlane, R. J.; Lee, B.; Jones, M. R.; Harris, N.; Schatz, G. C.; Mirkin, C. A., Nanoparticle Superlattice Engineering with DNA. **2011**, *334* (6053), 204-208.
38. Vo, T.; Venkatasubramanian, V.; Kumar, S.; Srinivasan, B.; Pal, S.; Zhang, Y. G.; Gang, O., Stoichiometric control of DNA-grafted colloid self-assembly. *P Natl Acad Sci USA* **2015**, *112* (16), 4982-4987.
39. Zhang, Y.; Lu, F.; Yager, K. G.; van der Lelie, D.; Gang, O., A general strategy for the DNA-mediated self-assembly of functional nanoparticles into heterogeneous systems. *Nature Nanotechnology* **2013**, *8*, 865.
40. Jones, M. R.; Seeman, N. C.; Mirkin, C. A., Programmable materials and the nature of the DNA bond. *Science* **2015**, *347* (6224), 1260901.
41. Mason, J. A.; Laramy, C. R.; Lai, C.-T.; O'Brien, M. N.; Lin, Q.-Y.; Dravid, V. P.; Schatz, G. C.; Mirkin, C. A., Contraction and Expansion of Stimuli-Responsive DNA Bonds in Flexible Colloidal Crystals. *J Am Chem Soc* **2016**, *138* (28), 8722-8725.
42. Zhang, Y.; Pal, S.; Srinivasan, B.; Vo, T.; Kumar, S.; Gang, O., Selective transformations between nanoparticle superlattices via the reprogramming of DNA-mediated interactions. *Nature materials* **2015**, *14* (8), 840-847.
43. Pal, S.; Zhang, Y.; Kumar, S. K.; Gang, O., Dynamic Tuning of DNA-Nanoparticle Superlattices by Molecular Intercalation of Double Helix. *J Am Chem Soc* **2015**, *137* (12), 4030-4033.

44. Tan, S. J.; Kahn, J. S.; Derrien, T. L.; Campolongo, M. J.; Zhao, M.; Smilgies, D. M.; Luo, D., Crystallization of DNA-Capped Gold Nanoparticles in High-Concentration, Divalent Salt Environments. *Angew Chem Int Edit* **2014**, *53* (5), 1316-1319.
45. Rubinstein, M.; Colby, R. H., *Polymer physics*. Oxford university press New York: 2003; Vol. 23.
46. Daoud, M.; Cotton, J., Star shaped polymers: a model for the conformation and its concentration dependence. *J Phys-Paris* **1982**, *43* (3), 531-538.
47. Srivastava, S.; Nykypanchuk, D.; Fukuto, M.; Gang, O., Tunable Nanoparticle Arrays at Charged Interfaces. *Acs Nano* **2014**, *8* (10), 9857-9866.
48. Srivastava, S.; Nykypanchuk, D.; Maye, M. M.; Tkachenko, A. V.; Gang, O., Super-compressible DNA nanoparticle lattices. *Soft Matter* **2013**, *9* (44), 10452-10457.
49. Borsali, R.; Nguyen, H.; Pecora, R., Small-angle neutron scattering and dynamic light scattering from a polyelectrolyte solution: DNA. *Macromolecules* **1998**, *31* (5), 1548-1555.
50. Brunet, A.; Tardin, C.; Salome, L.; Rousseau, P.; Destainville, N.; Manghi, M., Dependence of DNA Persistence Length on Ionic Strength of Solutions with Monovalent and Divalent Salts: A Joint Theory-Experiment Study. *Macromolecules* **2015**, *48* (11), 3641-3652.
51. Bosco, A.; Camunas-Soler, J.; Ritort, F., Elastic properties and secondary structure formation of single-stranded DNA at monovalent and divalent salt conditions. *Nucleic Acids Res* **2014**, *42* (3), 2064-2074.
52. Yu, J.; Mao, J.; Yuan, G. C.; Satija, S.; Jiang, Z.; Chen, W.; Tirrell, M., Structure of Polyelectrolyte Brushes in the Presence of Multivalent Counterions. *Macromolecules* **2016**, *49* (15), 5609-5617.
53. Willott, J. D.; Murdoch, T. J.; Leermakers, F. A. M.; de Vos, W. M., Behavior of Weak Polyelectrolyte Brushes in Mixed Salt Solutions. *Macromolecules* **2018**, *51* (3), 1198-1206.
54. Nap, R. J.; Szleifer, I., Effect of calcium ions on the interactions between surfaces end-grafted with weak polyelectrolytes. *J Chem Phys* **2018**, *149* (16).
55. Jiang, T.; Wu, J. Z., Ionic effects in collapse of polyelectrolyte brushes. *J Phys Chem B* **2008**, *112* (26), 7713-7720.
56. Borisov, O.; Zhulina, E. J. T. E. P. J. B.-C. M.; Systems, C., Effects of ionic strength and charge annealing in star-branched polyelectrolytes. **1998**, *4* (2), 205-217.
57. Zhulina, E.; Borisov, O.; Birshtein, T. J. M., Polyelectrolyte brush interaction with multivalent ions. **1999**, *32* (24), 8189-8196.
58. Muthukumar, M., *Polymer translocation*. CRC press: 2016.
59. Li, W. F.; Nordenskiold, L.; Zhou, R. H.; Mu, Y. G., Conformation-dependent DNA attraction. *Nanoscale* **2014**, *6* (12), 7085-7092.
60. Butler, J. C.; Angelini, T.; Tang, J. X.; Wong, G. C. L., Ion multivalence and like-charge polyelectrolyte attraction. *Phys Rev Lett* **2003**, *91* (2).
61. Tong, K.; Song, X.; Sun, S.; Xu, Y.; Yu, J. J. M. P., Molecular dynamics study of linear and comb-like polyelectrolytes in aqueous solution: effect of Ca²⁺ ions. **2014**, *112* (16), 2176-2183.
62. Luan, B.; Aksimentiev, A., DNA Attraction in Monovalent and Divalent Electrolytes. *J Am Chem Soc* **2008**, *130* (47), 15754-+.
63. Zhang, Z. L.; Wu, Y. Y.; Xi, K.; Sang, J. P.; Tan, Z. J., Divalent Ion-Mediated DNA-DNA Interactions: A Comparative Study of Triplex and Duplex. *Biophysical Journal* **2017**, *113* (3), 517-528.
64. Srivastava, A.; Timsina, R.; Heo, S.; Dewage, S. W.; Kirmizialtin, S.; Qiu, X. Y., Structure-guided DNA-DNA attraction mediated by divalent cations. *Nucleic Acids Res* **2020**, *48* (13), 7018-7026.
65. Dai, L.; Mu, Y. G.; Nordenskiold, L.; van der Maarel, J. R. C., Molecular dynamics simulation of multivalent-ion mediated attraction between DNA molecules. *Phys Rev Lett* **2008**, *100* (11).
66. Qiu, X. Y.; Parsegian, V. A.; Rau, D. C., Divalent counterion-induced condensation of triple-strand DNA. *P Natl Acad Sci USA* **2010**, *107* (50), 21482-21486.
67. Hill, H. D.; Millstone, J. E.; Banholzer, M. J.; Mirkin, C. A., The Role Radius of Curvature Plays in Thiolated Oligonucleotide Loading on Gold Nanoparticles. *Acs Nano* **2009**, *3* (2), 418-424.

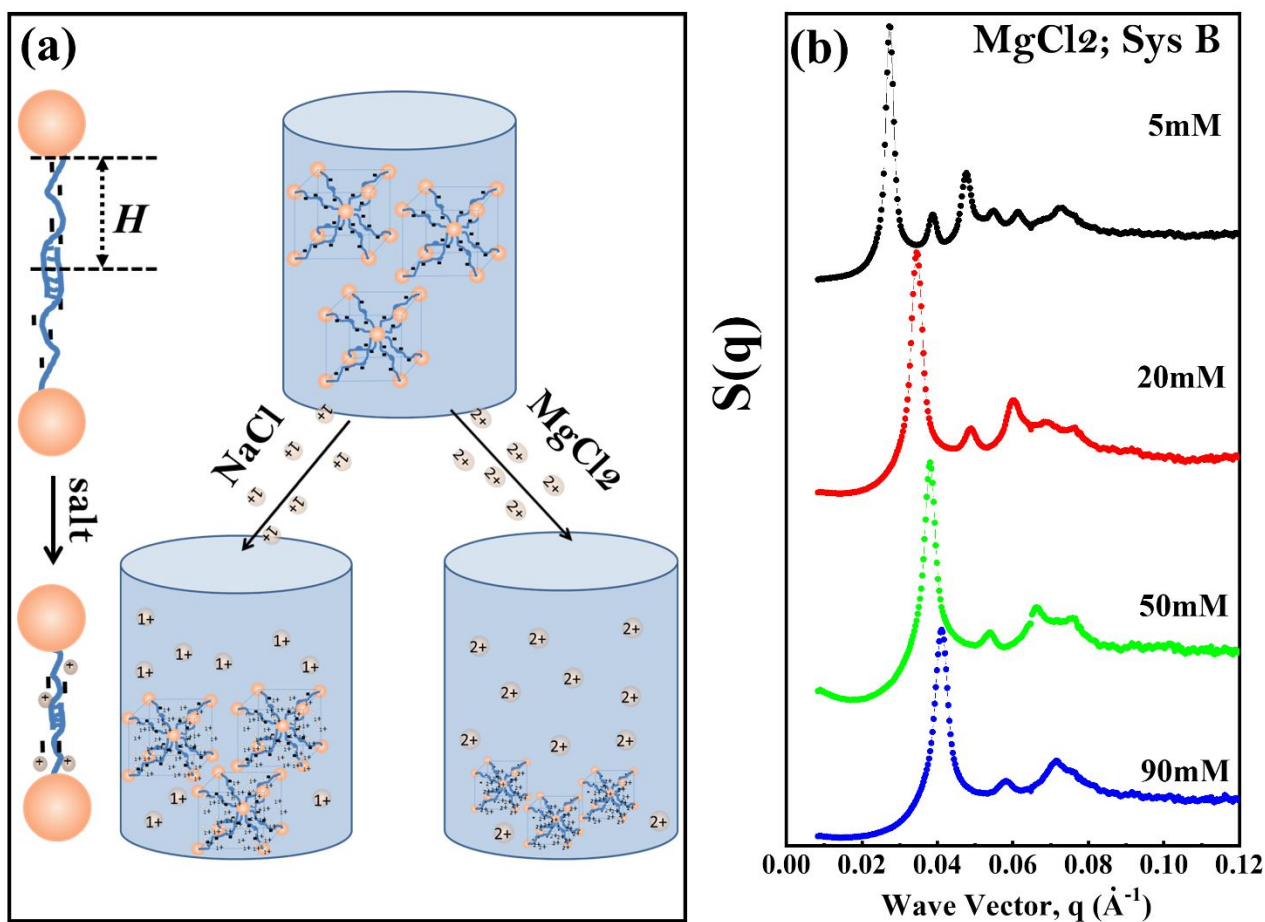


Figure 1: On overall design of the system and measurements (a) Schematic representation of the DNA chains linking nanoparticles (NP) and BCC DNA-NP superlattice for monovalent, NaCl and divalent, MgCl_2 , salt environments. (b) SAXS measured structure factor, $S(q)$, for Sys B for increased concentration of divalent salt. The shift of x-ray scattering peaks towards a higher q indicates a lattice shrinkage with a salt concentration increase.

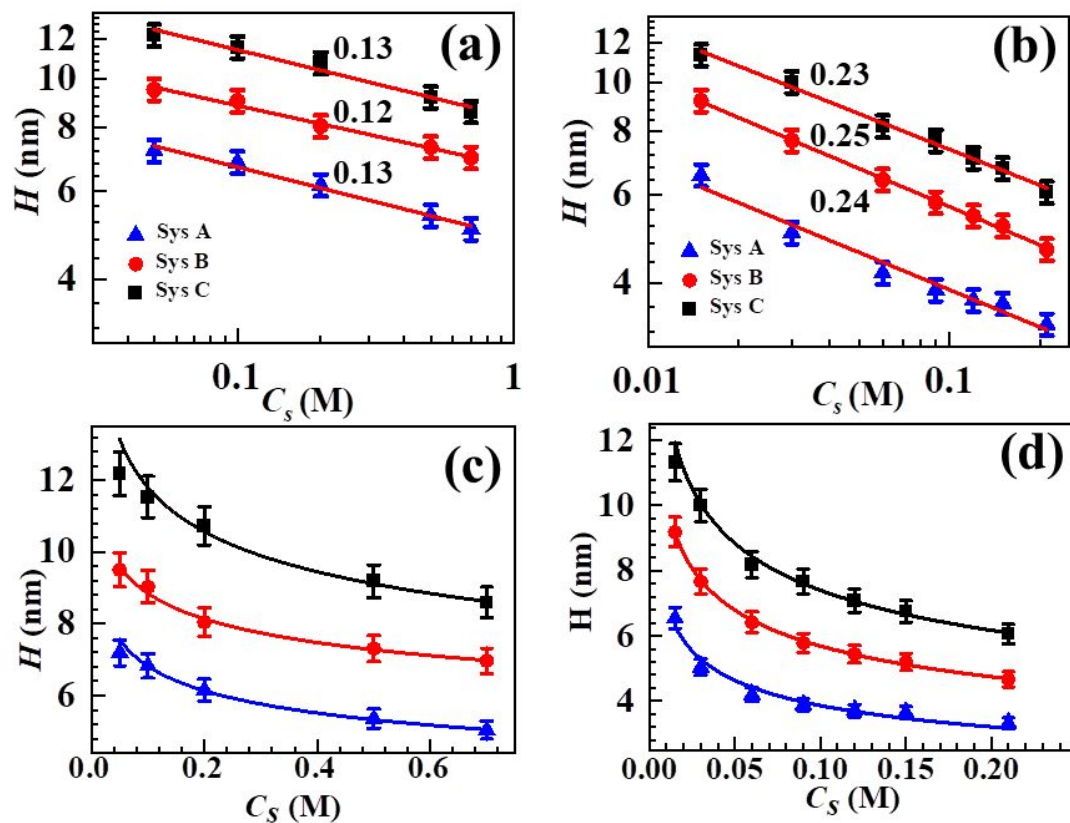


Figure 2: Brush length (H) at varying ionic strength, C_s , for (a,c) monovalent and (b,d) divalent salts. The estimates of the power law exponent, α , are indicated along-side each system (a,b) The corresponding symbols used for various systems are identical in all plots. The measured $H(C_s)$ dependence and a fit using a modified Daoud-Cotton model for discussed systems (A , B , C) for (c) monovalent (NaCl) and (d) divalent ($MgCl_2$) salts. Solid lines are fit to the data using the equation 1 in the main text.

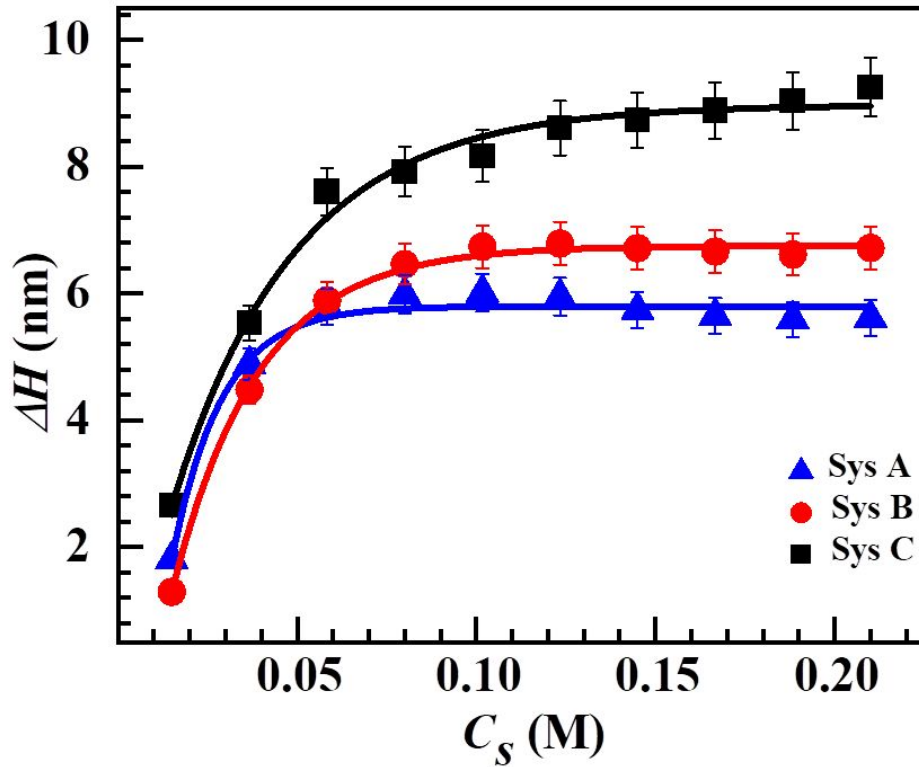


Figure 3: The difference in DNA brush length , $\Delta H = (H_{monovalent} - H_{divalent})$ as a function of ionic strength, C_s . The exponential growth function has been used to fit the experimental data in order to estimate the saturation value for salt concentration.

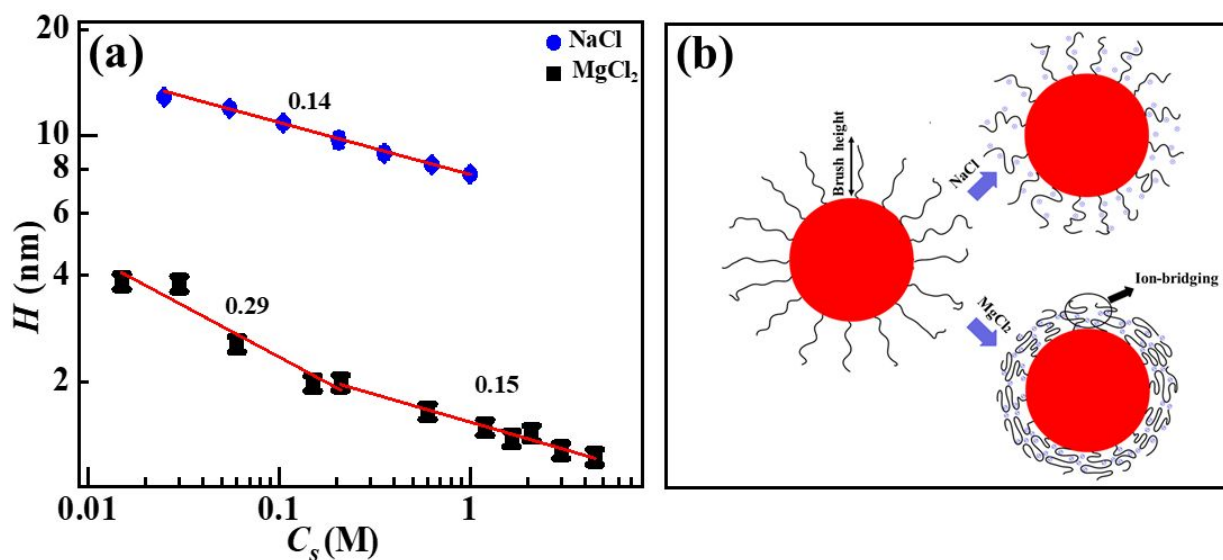


Figure 4: The behaviour of a brush length, H , at the different salt environments (a) H vs C_s for Sys B for added cationic salt as indicated. A power law exponent of 0.29 is measured with cross-over at ~ 0.2 M to value of 0.15, similar to that of monovalent systems. (b) Schematics of morphology of DNA grafted to nanoparticle surface in the presence of added monovalent and divalent salts. A cation mediated attraction leads to ion-bridging in case of a divalent salt ($MgCl_2$).